The Journal of Chemical Physics

Molecular dynamics simulation of cancer cell membrane perforated by shockwave induced bubble collapse

Cite as: J. Chem. Phys. **157**, 225102 (2022); https://doi.org/10.1063/5.0105675
Submitted: 24 June 2022 • Accepted: 28 November 2022 • Accepted Manuscript Online: 29 November 2022 • Published Online: 13 December 2022

Nguyen Hoang Linh, Viet Hoang Man, Mai Suan Li, et al.

The Journal of Chemical Physics ARTICLE scitation.org/journal/jcp

Molecular dynamics simulation of cancer cell membrane perforated by shockwave induced bubble collapse

Cite as: J. Chem. Phys. 157, 225102 (2022); doi: 10.1063/5.0105675
Submitted: 24 June 2022 • Accepted: 28 November 2022 •
Published Online: 13 December 2022

Nguyen Hoang Linh,[1] Viet Hoang Man,[2] Mai Suan Li,[1,3] Junmei Wang,[2] Philippe Derreumaux,[4,5] Thi Ly Mai,[5] and Phuong H. Nguyen[5,a)]

AFFILIATIONS

[1] Institute for Computational Science and Technology, SBI Building, Quang Trung Software City, Tan Chanh Hiep Ward, District 12, Ho Chi Minh City, Vietnam
[2] Department of Pharmaceutical Sciences, School of Pharmacy, University of Pittsburgh, Pittsburgh, Pennsylvania 15213, USA
[3] Institute of Physics, Polish Academy of Sciences, Al. Lotnikow 32/46, 02-668 Warsaw, Poland
[4] Institut Universitaire de France (IUF), Paris, France
[5] CNRS, Université Paris Cité, UPR 9080, Laboratoire de Biochimie Théorique, Institut de Biologie Physico-Chimique, Fondation Edmond de Rothschild, 13 rue Pierre et Marie Curie, 75005 Paris, France

[a)] **Author to whom correspondence should be addressed:** nguyen@ibpc.fr

ABSTRACT

It has been widely accepted that cancer cells are softer than their normal counterparts. This motivates us to propose, as a proof-of-concept, a method for the efficient delivery of therapeutic agents into cancer cells, while normal cells are less affected. The basic idea of this method is to use a water jet generated by the collapse of the bubble under shockwaves to perforate pores in the cell membrane. Given a combination of shockwave and bubble parameters, the cancer membrane is more susceptible to bending, stretching, and perforating than the normal membrane because the bending modulus of the cancer cell membrane is smaller than that of the normal cell membrane. Therefore, the therapeutic agent delivery into cancer cells is easier than in normal cells. Adopting two well-studied models of the normal and cancer membranes, we perform shockwave induced bubble collapse molecular dynamics simulations to investigate the difference in the response of two membranes over a range of shockwave impulse 15–30 mPa s and bubble diameter 4–10 nm. The simulation shows that the presence of bubbles is essential for generating a water jet, which is required for perforation; otherwise, pores are not formed. Given a set of shockwave impulse and bubble parameters, the pore area in the cancer membrane is always larger than that in the normal membrane. However, a too strong shockwave and/or too large bubble results in too fast disruption of membranes, and pore areas are similar between two membrane types. The pore closure time in the cancer membrane is slower than that in the normal membrane. The implications of our results for applications in real cells are discussed in some details. Our simulation may be useful for encouraging future experimental work on novel approaches for cancer treatment.

I. INTRODUCTION

The plasma cell membrane regulates the entry and exit of substances via specific mechanisms. Small substances, such as ions, sugars, and amino acids, can cross the membrane via ion channels or protein pumps. Macromolecules must be carried into cells by membrane bound vesicles through the endocytosis mechanism.[1] These two mechanisms limit the entry of molecules, which are not naturally needed by cells. As a consequence, although a large number of drugs are available for treating cell diseases, only a few drugs are used if they can cross the cell membrane. Therefore, a number of approaches have been proposed, aimed at enhancing the transport of drugs through the cell membrane. Two well-known viral and chemical methods have been developed, but they are still limited by low efficiency and toxicity. As a remedy, the physical approach has been recently proposed for a highly efficient drug delivery with low toxicity. The basic idea of the physical approach is to create transient pores in the cell membrane, called poration,

where drugs can penetrate into cells easier. Physical methods include photoporation, electroporation, magnetoporation, and mechanoporation, which use different kinds of physical forces, such as magnetic, thermal, mechanical, and electrical forces to open the pore. For an excellent review of the drug delivery methods, readers are referred to the recent publication.[2] Among these methods, mechanoporation using the shockwave force is promising because it can rapidly deliver large macromolecules into cells in a local, noninvasive, and cost-effective manner.[3] For examples, Kodama *et al.* used shockwaves to deliver large cytoplasmic molecules into cells. The authors suggested that the shear force generated by the shockwave temporarily affects the permeability of the membrane, and the impulse of the shockwave plays an important role in governing the permeability. This method can deliver large macromolecules of up to 2×10^6 molecular weight into cells.[4] Recently, López-Marín *et al.* have studied the shockwave induced damage and poration in cell line HEK293 and tumor-derived cell line MCF-7, and the results from scanning electron microscopy revealed transient hole-like structures after shockwave exposure. The authors also showed differences in the membrane permeability of two cell lines.[5] Qi *et al.* showed that shockwaves can trigger the release of adenosine triphosphate (ATP) from osteosarcoma U2OS cells by increasing the membrane permeability.[6] The ability of shockwaves to enhance the delivery of very large molecules suggests that shockwaves should also be a promising method in gene therapy and protein delivery.[7,8] We should mention that the shockwave has been used in other medical applications. For example, high energy shockwaves have been used for more than 30 years to disintegrate urolithiasis. Extracorporeal shockwave therapy has been clinically used for many musculoskeletal conditions. It has been suggested that the shockwave accelerates tissues regeneration, reduces calcification, and inhibits pain receptors.[9]

To further develop this sensitive method aimed at enhancing drug delivery into cancer cells, one needs a better understanding of the mechanism of shockwaves interacting with the cell membrane, especially at the molecular level. Unfortunately, it is very difficult to experimentally observe the direct interaction between shockwaves and membranes due to the short time scale on the order of picoseconds and small length scale of several nanometers. Therefore, several studies have employed molecular dynamics (MD) simulations to investigate the molecular mechanism of the shockwave induced membrane damages with and without bubbles.[10–23] Koshiyama *et al.* performed for the first time an all-atom nonequilibrium MD simulation under a shockwave but without bubbles and observed the penetration of waters into the hydrophobic region of the membrane, which was caused by a decrease in membrane thickness.[10] Choubey *et al.* performed large-scale all-atom MD simulations of lipid membranes with shockwaves and nanobubbles and showed that the bubble collapse generates shear flow of water on membrane leaflets and pressure gradients across them, creating transient nanochannels through which water molecules translocate across the membrane.[11] Steinhauser and colleagues developed an advanced large and multi-scales coarse-grained simulation method using dissipative particle dynamics and applied it to study effects of shockwaves on 1,2-dipalmitoylphosphatidylcholine (DPPC) membranes. The authors obtained a threshold shock front velocity, below which the membrane recovers from shockwave induced damage and above that the membrane could not be recovered.[12–15] Santo and Berkowitz employed coarse-grained MD simulation to study the impact of shockwaves and bubbles on the damage and recovery of lipid membranes. Interestingly, they showed that not every lipid molecule remained in the bilayer after recovery, some lipids moved out into water and created micelles.[16,17] Adhikari *et al.* showed that in the absence of bubbles, high intensity shockwaves do not induce pores on membranes, but weaker impulses can lead to membrane poration in the presence of bubbles.[18] Similarly, Lu *et al.* performed MD simulation of the shockwave induced delivery of paclitaxel drug through a lipid membrane and showed that the paclitaxel molecule can penetrate the membrane only under the joint effect of the shockwave and nanobubble.[20] Sun *et al.* simulated the shockwave induced collapse of lipid-shelled nanobubbles, and interestingly, they showed that compared with the cases of vacuum nanobubbles, the lipid nanobubbles could weaken the effects of shock waves.[19] Nan *et al.* performed coarse-grained MD simulation of the shockwave induced bubble collapse and observed not only membrane perforation but also the occurrence of nanoscale cavitation during the perforation process.[21] Hu *et al.* analyzed effects produced by the collapse of multiple nanobubbles in the vicinity of biomembranes in the presence of an electric field by MD simulation[22] and showed that multiple nanobubbles make it possible to create larger pores on the membrane.[22] Very recently, Wei *et al.* have studied the impact of the shockwave induced bubble collapse on the damage of cell membranes with different lipid peroxidation levels and have shown that the pore sizes increase with the peroxidation level.[23] One of the important findings obtained from all these simulation studies is that the shockwave alone does not have much impact on membranes, but the presence of gas bubbles, which pre-exist or are nucleated during the shockwave propagation, plays an essential role in the membrane poration.

Our main interest is the application of the shockwave in combination with bubbles in the drug delivery for cancer treatment. To date, cancer treatments, including surgery, radiotherapy, and chemotherapy, are widely used. Extensive resection followed by adjuvant chemo-radiotherapy seems to be the only treatment that modifies the survival of cancer patients. However, with chemotherapy, the therapeutic agent affects not only cancer cells but also normal cells, causing severe side effects. Therefore, novel therapeutic methods are needed to minimize side effects on the normal cells. Our core aim is to develop such a method based on the difference in the mechanical properties of normal and cancer membranes. Recently, a number of studies have shown that cancer cells from a large number of different organs are softer than their normal counterparts.[24] Therefore, in recent years, mechanical properties of cancer cells have been suggested as biomarkers for early cancer diagnosis, targeted for the prediction, treatment, and even prevention of cancer.[25] Our research hypothesis is that if cancer cells are softer than normal cells, then we can choose shockwaves with appropriate impulses and bubbles with suitable sizes so that under the shockwave induced bubble collapse, the cancer cell membrane is maximally perforated, while the normal cell membrane is minimally affected. Therefore, therapeutic agents are maximally delivered into cancer cells but minimally into normal cells.

In a previous work, we performed equilibrium MD simulations to study the elastic properties of normal cell membranes and cancer cell membranes.[26] In our simulation models, normal cell membranes have a highly asymmetric lipid composition,[27] where the extracellular leaflet is mainly composed of phosphatidylcholine (PC) and

sphingolipids and the intracellular leaflet is mostly composed of phosphatidylethanolamine (PE) and phosphatidylserine (PS) lipids. When normal membranes are transformed to cancer membranes, the concentration of the negatively charged PS lipids is increased in the extracellular leaflet[28,29] and the cholesterol (CHL) concentration is reduced.[30] We calculated the elastic moduli, including bending, tilt, and twist constants of the normal and cancer membranes. The results showed that at low cholesterol concentrations, all elastic moduli become smaller, implying that the cancer membrane is indeed softer than the normal counterpart.

In this work, we carry out nonequilibrium MD simulations of the shockwave induced bubble collapse of a normal membrane and a cancer membrane whose structures are known from our previous work.[26] We vary the shockwave impulses and bubble diameters over a wide range of values to observe the difference in the response of the normal and cancer membranes. The main finding is that given a combination of a shockwave and a bubble, the cancer membrane is more bent, stretched, and perforated than the normal counterpart.

II. METHODOLOGY

A. The membrane models

In a previous work,[26] we carried out all-atom MD simulations of five normal membrane models and five cancer membrane models. The cancer membranes took into account the overexpression of PS lipids in the outer leaflet and the reduction of cholesterol concentration. Results showed that at the same cholesterol concentration, the bending moduli of the normal and cancer membranes are very similar. This indicates that the overexpression of the PS lipids does not significantly affect the elasticity of the normal or cancer membranes. At low cholesterol concentrations, all elastic moduli become smaller, implying that the reduction in cholesterol in cancer membranes could contribute at least partly to the softening of cancer cells. Therefore, in this work, we consider only two membrane models among the ten membrane models used in previous work:[26] a normal membrane model and a cancer membrane model, which differ in the PS lipid concentration in the outer leaflets and in the cholesterol concentration. Each model contains four lipid types: 1,2-dioleoyl-sn-glycero-3-phosphocholine (DOPC), sphingomyelin lipids (SM), 1,2-dioleoyl-sn-glycero-3-phosphoethanolamine (DOPE), and 1,2-dioleoyl-sn-glycero-3-phospho-L-serine (DOPS) lipids. For each model, we take the last equilibrium membrane structure at 2 μs obtained from previous simulations[26] and translate it along the x and y axis to obtain a doubled size membrane with lengths $(x, y) = (24, 24)$ nm. This guarantees that the new membrane structure is in the equilibrium state and large enough to accommodate large bubbles having diameters of ~10 nm. The numbers of lipids and cholesterol of two membrane models are listed in Table I.

TABLE I. The total number of each lipid component in the outer and inner leaflets of the normal and cancer membrane models. The cancer membrane model is obtained by symmetrizing the number of lipids between the outer and inner leaflets of the normal membrane model.

	Normal membrane		Cancer membrane	
Lipid	Outer	Inner	Outer	Inner
SM	336	96	216	216
DOPC	368	112	240	240
DOPE	112	368	240	240
DOPS	0	240	120	120
CHL	408	408	204	204

B. Shockwave induced bubble collapse simulation method

In this work, we employ the shockwave method originally developed by Koshiyama *et al.*[10] The sketch of the simulation setup is shown in Fig. 1. The system is a rectangular prism box composed of two lipid membranes described above and a bubble, and the whole system is solvated in water. We are interested in the lower membrane, while the upper membrane is only technically used to prevent the shockwave coming back to another side of the lower membrane due to the periodic boundary condition used in simulation.[31,32] The distance between the membrane and the bubble is d_{mb}, and the diameter of the bubble is d_b. To generate a shockwave with an impulse I, an excess momentum $M = I \times A$ is applied to a slab of waters with a volume of $A \times d_s$. Here, A and d_s are the area in the (x, y) plane and the thickness of the water slab, respectively. Initially, the distance between the slab of water and the bubble is d_{bs}.

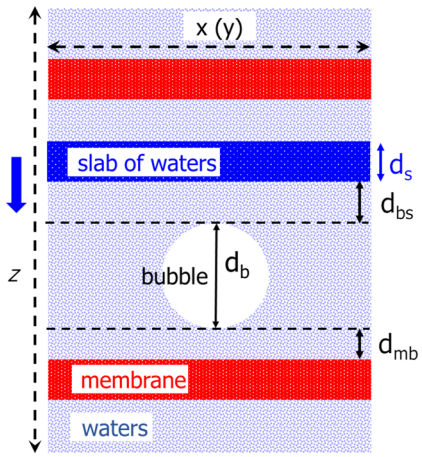

FIG. 1. Sketches of the shockwave induced bubble collapse simulation method. The rectangular prism box with lengths (x, y, z) contains two membranes and a bubble solvated in water. A slab of waters with a volume of $x \times y \times d_s$ is selected for the shockwave generation. A bubble with a diameter d_b is placed at a distance of d_{mb} above the membrane. The distance between the water slab and the bubble is d_{bs}.

The all-atom CHARMM36 force field[33] and the TIP3P water model are used to model the lipids and solvent, respectively. The initial dimensions of the primary unit cell are $(x, y, z) = (24, 24, 54)$ nm, consisting of 3.112.724 atoms in total. Starting from the initial structure of the normal membrane or cancer membrane, an equilibrium MD simulation is carried out for 100 ns in the NPT ensemble at the pressure $P_0 = 1$ bar and temperature $T = 300$ K. Then, we take the last ten equilibrium structures separated by 100 ps, and for each structure, we remove water molecules in the spherical region having diameter d_b near the lower membrane. This empty water space mimics a bubble. In this work, we consider four bubble sizes with

d_b = 4, 6, 8, 10 nm. These membrane/bubble systems are used as initial structures for shockwave simulations. The shockwave I defined as the time integral of pressure over the shock pulse duration is varied from I = 15 mPa s to I = 25 mPa s. The shockwave induced bubble collapse MD simulation is performed by using the GROMACS simulation package[34] in the NVE ensemble. The equations of motion are integrated using the leapfrog algorithm with a small time step of 0.5 fs. The small time step is used to ensure the stability of simulations. The electrostatic interactions are calculated using the particle mesh Ewald method, and a cutoff of 1.2 nm[35] and the forces switched to zero from 1.0 to 1.2 nm are used for the van der Waals interactions. The nonbonded pair lists are updated every 5 fs. Each simulation is run for 50 ps, and the data are saved for every 500 MD steps (every 0.25 ps) for subsequent analyses.

C. Data analysis

In our simulations, the shockwave moves in the z-direction; thus, to monitor the propagation, we calculate profiles of the normal pressure component, $P_{zz}(z)$, and temperature, $T(z)$. To this end, we discretize the simulation box in thin slabs of width 0.5 nm, which are oriented parallel to the xy-plane. By computing the average pressure and temperature in each slab, the propagation of can be monitored in detail. Here, pressure is calculated by using the method developed by Ollila *et al.*,[36] and temperature is directly calculated from the velocity of atoms.

To measure the membrane pore area ΔS, we place a 2D grid with the size of each grid square of (0.1×0.1) nm^2 on the (x, y) membrane surface and count the squares on the grid having zero lipid atoms.[18,23]

The order parameters of the lipid acyl chain tails are calculated as $S_i = \langle 3\cos^2\theta_i - 1\rangle/2$, where θ_i is the angle between the ith C–H bond vector and the bilayer normal,[37] and the angular brackets represent the ensemble average over all lipids.

III. RESULTS

We have performed MD simulations to investigate the difference in the response of the normal and cancer cell membranes to the shockwave induced bubble collapse. There are five parameters in the simulation setup, including the shockwave impulse I, diameter of bubble d_b, distance from bubble to membrane d_{mb}, distance from water slap to bubble d_{bs}, and thickness of water slap d_s (Fig. 1). Among these, two physical parameters that can be controlled experimentally are the shockwave impulse I and bubble size d_b. The other parameters d_{mb}, d_{bs}, d_s are merely parameters defined only in simulation. Thus, in this study, we only choose appropriate values, d_{mb} = 1 nm, d_{bs} = 2 nm, and d_s = 3 nm, for all simulations, and values of I and d_b are varied to obtain different responses in the membranes. We note that two membranes are used in simulations, but as explained above, we are only interested in the lower membrane (Fig. 1) whose results are presented below. For each simulation, ten trajectories are carried out starting from different initial structures, and the results are presented as an ensemble average over all trajectories.

A. Shockwave induced bubble collapse and membrane response

To describe the shockwave propagation, the collapse of the bubble, and the response of the membrane in detail, let us consider a representative simulation of the normal membrane using a shockwave impulse I = 21 mPa s and a bubble with diameter d_b = 10 nm. We calculate various quantities, including the vector field of the velocity of atoms and the profiles of the pressure, kinetic energy, temperature, and mass density. To provide an intuitive picture, snapshots are also visualized. These results are shown in Figs. 2 and 3.

By construction, all atoms within the water slab above the bubble (Fig. 1) are initially assigned to the same high velocity V, which is calculated as $V = (I \times A)/(m \times N)$.[10] With the impulse I = 21 mPa s, the area of the water slab A = 576 nm^2, the weight of a water molecule m = 18 g/mol, and the number of water molecules in that slab N = 58 044, we obtain $V \sim 9$ km/s with the direction parallel to the z axis and toward the membrane. This results in an excess high temperature of ~15 000 K and a pressure of ~44 GPa in the water slab at t = 0 ps [Figs. 2(a) and 2(b)]. These water atoms then move extremely fast toward the membrane as seen from the velocity vector field in Fig. 3(a). This causes an increase in the water density profile in the direction of the membrane with the maximum values of 1532 kg/m^3 at $t \sim 1.25$ ps, $z \sim 21$ nm and 1519 kg/m^3 at $t \sim 3$ ps, $z \sim 15$ nm, thus leaving an empty space behind them at the initial position of water slab ($z \sim 30$ nm) [Figs. 2(c) and 3(b)]. This is because the initially equilibrated water molecules at 300 K above the water slab are not quick enough to occupy the space left by the water in the slab. As a consequence, the temperature and pressure in the water slab are reduced significantly from the initial values and increased quickly in the direction of the membrane, reaching the maximum values of ~3400 K and 20 GPa, respectively, at $t \sim 1.25$ ps and $z \sim 21$ nm [Figs. 2(a) and 2(b)]. Along the way, a part of water in the slab enters the empty space of the bubble without any obstacle, mimicking the bubble collapse. At t = 1.25 ps, the bubble is

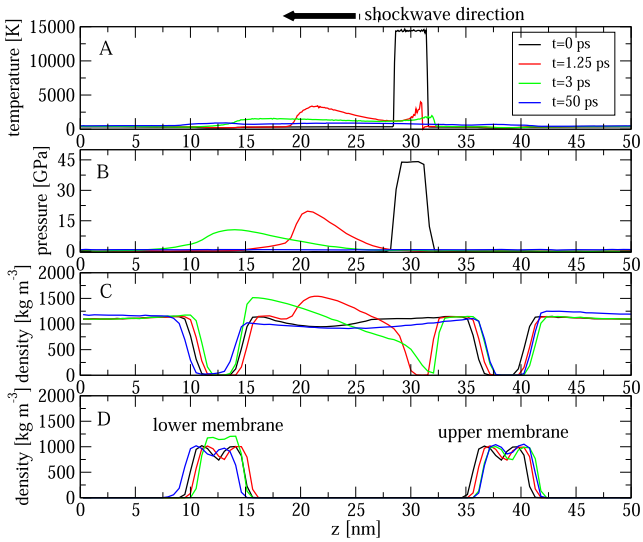

FIG. 2. The profiles along the z axis of the temperature (a), normal pressure component (b), mass density of water (c), and mass density of membrane (d) obtained at 0 ps (black), 1.25 ps (red), 3 ps (green), and 50 ps (blue). Results obtained from the simulation of the normal membrane using a shockwave impulse I = 21 mPa s and a 10 nm bubble are shown.

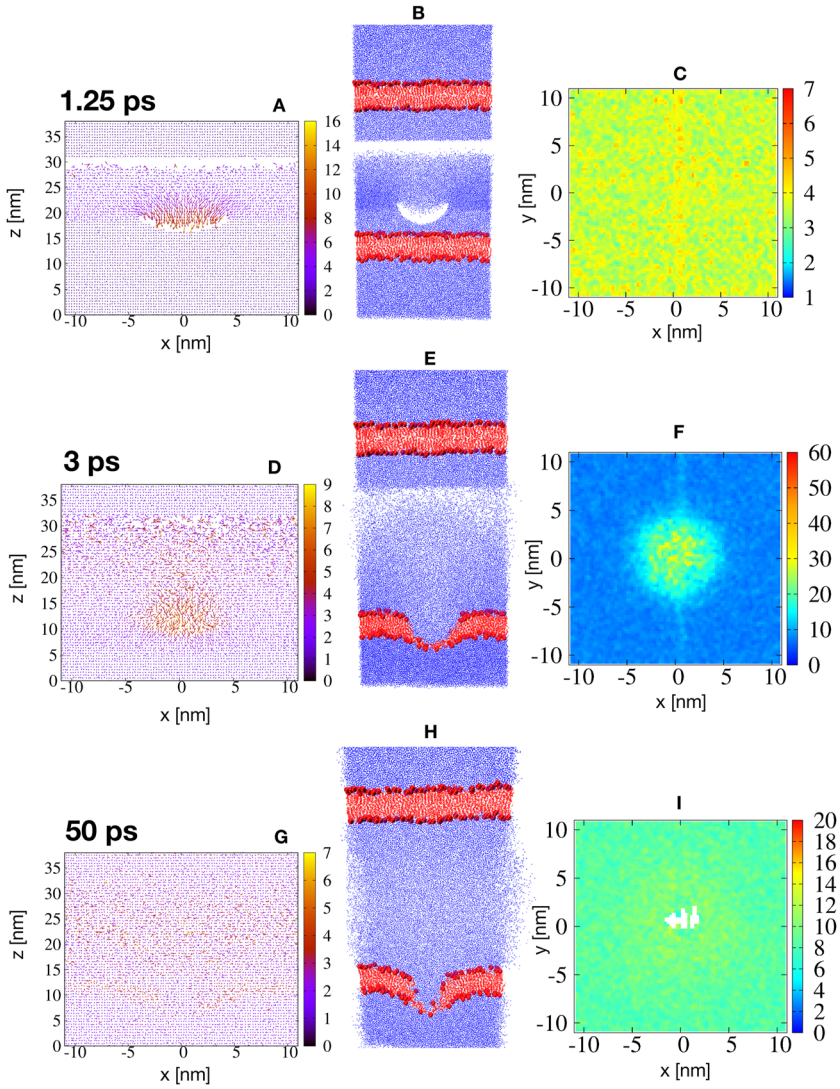

FIG. 3. The velocity field (in km/s) of atoms projected on the (*x*, *z*) plan [(a), (d), and (g)]; the snapshot of the system [(b), (e), and (h)]; and the kinetic energy (in kJ/mol) map of atoms projected on the (*x*, *y*) plan [(c), (f), and (i)]. Results at 1.25, 3, and 50 ps for the normal membrane simulated with a shockwave impulse of 21 mPa and a 10 nm in diameter bubble are shown. In the snapshots, the water and membrane are shown in blue and red colors, respectively. The white area in (i) indicates the pore.

partially collapsed [Fig. 3(b)], but the membrane has not been affected yet; thus, the average kinetic energy of the membrane is still maintained at an equilibrium value of ~4–5 kJ/mol, uniformly distributed over all lipids [Fig. 3(c)], and the temperature is still around the initial value of ~300 K [Fig. 2(a)]. In contrast, the propagation of the part of waters in the slab, which do not enter the bubble, is slower due to the resistance of the water below the slap. The difference in the velocity between these two arts of water, i.e., one enters the bubble and one outside the bubble, produces a high-speed water jet directed toward the membrane, as shown by the velocity vector field in Fig. 3(a). After entering the bubble, the water jet continues to propagate and occupies completely the bubble space at $t \sim 3$ ps, mimicking the full collapse of the bubble [Fig. 3(e)]. Then, it hits the lipid membrane and velocity drops down to ~6 km/s with the velocity vector field shown in Fig. 3(d). The membrane area located just below the bubble receives directly the kinetic energy from the water jet; thus, its temperature and pressure at the membrane surface [$z \sim 15$ nm, Fig. 2(d)] increase to ~1600 K and ~10 GPa, respectively [Figs. 2(a) and 2(b)], and the kinetic energy at the focal point of the membrane increases to ~40 kJ/mol [Fig. 3(f)]. The kinetic energy of the remaining part of the membrane is slightly increased to ~10 kJ/mol. This causes the deformation of the membrane area just below the bubble [Fig. 3(e)]. After that, the water jet is thermalized and its kinetic energy is redistributed, leading to an increase in the kinetic energy of ~14 kJ/mol of surrounding water and lipid molecules. Their velocities are randomly distributed, as shown by the velocity vector field and kinetic energy map in Figs. 3(g) and 3(i), respectively, at 50 ps. The membrane is now highly stretched, and pores are formed [Figs. 3(h) and 3(i)]. We note that the membrane is basically not translated under shockwaves as seen from the

position z of the membrane density profile shown in Fig. 2(d). This is due to the use of two membrane technique in our simulation as described above.

We also calculate the average temperature and normal pressure across the membrane surface as a function of time, and the results are shown in Fig. 4. The temperature remains at the initial value of ~300 K until the arrives. Upon the arrival, the temperature increases sharply to maximum values of ~700 K at ~5 ps, and then, it slowly decreases and reaches ~560 K at 50 ps. Similarly, there is a sharp increase in pressure from the initial value ~10^{-4} GPa (1 bar) to the maximum value of 4.2 GPa at ~5 ps, followed by a rapid decrease of pressure, which reaches a minimum value of ~0.35 GPa at 13 ps, and then, the pressure rises again toward the final value of ~0.73 GPa at 50 ps. We should mention that the shockwave induced bubble collapse simulation is carried out in the NVE ensemble, and the very high initial kinetic energy of the shockwave is redistributed over all atoms; thus, the temperature and pressure of the membrane do not relax to the initial values of 300 K and 1 bar, respectively. Of note, we analyzed trajectories simulated with different shockwave impulses and bubble sizes and found that the mechanism of bubble collapse and membrane response is similar for all simulations.

It is of interest to compare the targeted impulse I, which is used to generate the initial shockwave, with the actual pressure impulse exerted by the shockwave on the membrane. From the pressure profile $P(t)$ shown in Fig. 4, the pressure impulse on the membrane is calculated as $I_{\mathrm{mem}} = \int_0^t P(\tau)d\tau$, where t is the time duration of the positive phase of the shockwave.[10] The results are shown in Table II for simulations using a 10 nm bubble and different targeted impulses I. As seen, the actual pressure impulses are very close to the targeted counterparts, indicating that the initial impulses are not dissipated much before hitting the membrane. Therefore, the membrane is indeed impacted by the targeted impulses.

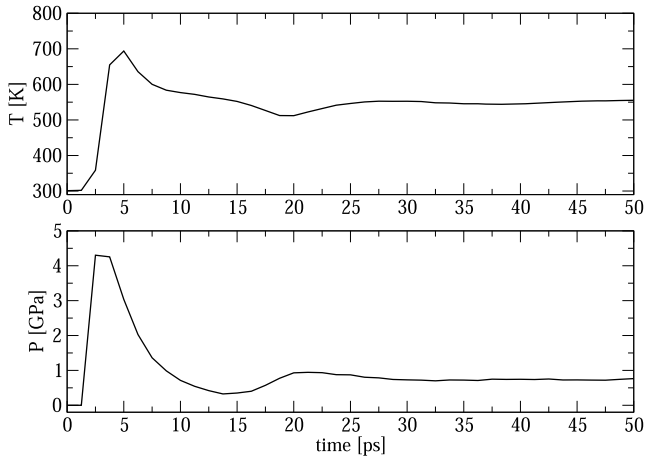

FIG. 4. Time dependence of the average temperature (upper panel) and normal pressure (lower panel) across the membrane surface along the z direction. Results obtained from the simulation of the normal membrane using a shockwave impulse I = 21 mPa s and a 10 nm bubble are shown.

TABLE II. A comparison between the targeted impulse I and the actual pressure impulse I_{mem} exerted on the membrane by the shockwave induced bubble collapse. v_{slab} is the initial velocity assigned to water atoms in the water slab for a given targeted impulse. In all cases, the time duration of the positive phase of the shockwave t = 10 ps is used in the calculation. Results obtained from simulations of the normal membrane using a 10 nm bubble are shown.

I (mPa s)	v_{slab} (km/s)	I_{mem} (mPa s)
15	6.43	13.18 ± 0.15
17	7.28	16.01 ± 0.21
19	8.14	17.90 ± 0.18
21	9.00	19.71 ± 0.23
23	9.85	22.05 ± 0.12
25	10.71	24.56 ± 0.26

B. Response of normal and cancer membranes upon bubble collapse

Having understood the mechanism of shockwave induced bubble collapse, we now wish to investigate the response of the normal and cancer membranes in detail, focusing on the membrane bending, lipid ordering, and membrane pore formation. In the previous simulation, we calculated the elastic moduli of the normal and cancer membranes in the equilibrium state and obtained the bending modulus $K_c = 10.5 \times 10^{-20}$ J for the normal membrane and $K_c = 8.1 \times 10^{-20}$ J for the cancer membrane.[26] This means that the cancer membrane is softer than the normal membrane. This implies that under the same water jet, the cancer membrane should be deformed more than the normal membrane. To confirm this, we carry out simulations using a 10 nm diameter bubble and a relatively weak shockwave of 15 mPa s such that only the membrane bending, but not pore formation, is observed. To obtain a qualitatively impression, Fig. 5 shows snapshots of the two membranes at t = 3 ps, and indeed, the cancer membrane is bent more than the normal membrane, with a bending of 2.0 and 1.2 nm, respectively.

To examine the response of membranes in more detail, we follow the time-evolution of the order parameters of the lipid acyl chain tails during the simulation of the normal and cancer membranes. For the DOPC, DOPE, and DOPS lipids, each

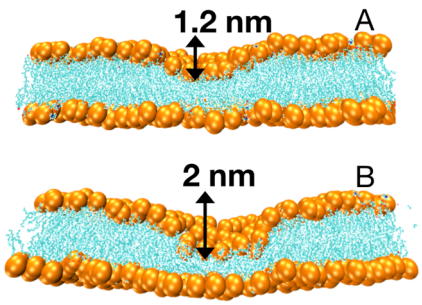

FIG. 5. Snapshots taken at t = 3 ps from the simulation of the normal (a) and cancer (b) membranes with a bubble having a diameter of 10 nm and a shockwave impulse of 15 mPa s. The phosphate atoms of lipids are shown in orange, and other atoms are shown in cyan. The bending values of the membranes are indicated.

tail consists of 17 order parameters ($i = 1, \ldots, 17$), and for SM lipids, each tail consists of 15 order parameters ($i = 1, \ldots, 15$). For simplicity, we sum all order parameters of each lipid type: $S_{lipid} = \sum_i S_i$. As an example, the time-evolution of the four S_{lipid} in the normal and cancer membranes is shown in Fig. 6 for the simulations using a 10 nm diameter bubble and a shockwave of 21 mPa s. As seen, both normal and cancer membranes are initially at equilibrium, and their order parameters are very similar. At $t \sim 3$ ps, the bubble is completely collapsed and the water jet hits the membrane. Thus, the membrane is highly disturbed and lipids become disordered. This is indicated by a largest reduction of ~60% in the order parameters of all lipid types at 3–4 ps for both membranes. Then, the intensity of the water jet is reduced because its kinetic energy is transferred to other degrees of freedom of the membrane and water. After hitting the lower membrane, the water molecules bounce back, and the membrane also tends to be pulled back to its original state as indicated by the increase in all order parameters of all lipid types from 3 to 18 ps. However, due to the presence of the upper membrane, the water molecules bounce back toward the lower membrane again, causing the lipids to become disordered as indicated by the decrease in order parameters at $t \sim 18$–20 ps. Then, the kinetic energy of the water molecules is redistributed, and the oscillation of the water flow between the upper and lower membranes disappears, the membrane is stabilized, and the order parameters approach horizontal values (see at 50 ps). Importantly, we observe that the cancer membrane is more disordered than the normal membrane. The order parameters of the cancer membrane are ~14% lower than those of the normal membrane (Fig. 6).

To see what changes in the structure of the membrane lead to a decrease in the order parameters S_i at ~3 ps seen in Fig. 6, we calculate the distribution of the θ_i angle between the ith C–H bond vector and the bilayer normal for different lipid types. We found that at equilibrium, these angles are mainly distributed around 0°; thus, S_i are large. Upon hit by the water jet around 3–4 ps, the distributions of θ_i are broader due to the compressed lipids, leading to smaller order parameters. Therefore, the reduction in the order parameters is associated with the reduction in the membrane thickness.

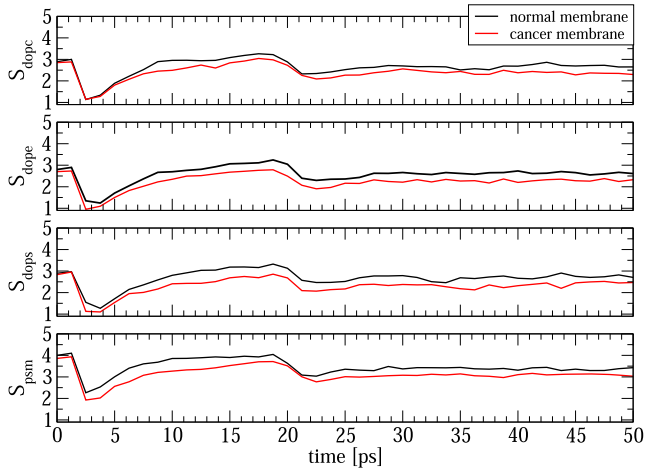

FIG. 6. Time-evolution of the sum lipid order parameter S_{lipid} of the normal (black) and cancer (red) membranes obtained from a simulation using a shockwave impulse of 21 mPa s and a bubble with a diameter of 10 nm.

The main aim of the shockwave induced bubble collapse method is to create pores on the cell membrane where drugs can be efficiently delivered into the cell. Therefore, the pore area is an important quantity to validate the efficiency of the method. We calculate the pore area ΔS (see Sec. II C) in the normal or cancer membrane at equilibrium and obtain an area of $\Delta S \sim 3$ nm^2. Of course, there is no well-defined pore in an equilibrium membrane, and this value is simply the sum of all small empty spaces in the (x, y) plane of a membrane at equilibrium.

First, we investigate the dependence of the pore area on the shockwave impulse, given a bubble size. Figure 7 shows, as an example, the time evolution of the pore area induced by the collapse of a 10 nm bubble under different shockwave impulses $I = 15$–25 mPa s for the normal and cancer membranes. Overall, the same feature of the time evolution of the pore area is observed for all impulses and for two membranes. At $t = 0$ ps, when the water jet has not hit the membrane yet, both membranes are at equilibrium and $\Delta S \sim 3$ nm^2. Then, the shockwave induces the collapse of the bubble and the generated water jet hits the membranes. With $I = 15$ mPa s, the water jet is not strong enough to perforate pores in the membrane. The membranes are slightly bent, as seen from Fig. 5, and ΔS is slightly above the equilibrium value. With $I = 17$ and 19 mPa s, the pore areas slowly increase and reach the largest values of 4–4.5 nm^2 around $t = 15$ ps. With stronger impulses of $I = 21$, 23, and 25 mPa s, the membranes are quickly perforated, and largest pore areas are formed around $t = 7$–10 ps. After that, the intensity of the water jet decreases and the pores tend to close, reflected by the decrease in pore areas. After 20 ps, the water jet is vanished, and the pores are fully closed as in the weak shockwave cases $I = 15$–19 mPa s. However, larger pores perforated by stronger shockwave impulses $I = 21$–25 mPa s are not closed after 50 ps. Clearly, for both membranes, the pore area increases with the increase of the shockwave impulse. For instance, at a low impulse intensity of 19 mPa s, the maximum pore area is around 4.5 nm^2, but with an intensity $I = 25$ mPa s, the pore area is three times larger, around 13 nm^2. We note that in all cases, largest pores are formed at $t \sim 10$–15 ps, while the maximum reduction in the lipid order parameter occurs much faster, around 3–4 ps (Fig. 6). To explain this, we note that the membrane outer leaflet (facing the water jet) is affected immediately upon hit by the water jet, while the inner leaflet has not been affected yet (Fig. 5). Thus, at this moment, the lipid order parameters, which are calculated for lipids pertaining in both leaflets, are affected. In contrast, a pore in a bilayer is fully formed only if pores are formed in both leaflets, and this process is slow.

At weak shockwave impulses $I = 15$–17 mPa s, there is no difference in ΔS between the normal and cancer membranes because in these cases, pores are not really formed. At $I = 19$ mPa s, the pore area in the cancer membrane is slightly larger than that in the normal membrane. The difference becomes more obvious with $I = 21$–23 mPa s, with the maximum pore areas in the cancer membrane being 19%–23% larger than those in the normal membrane. Interestingly, with $I = 25$ mPa s, the pore areas in both membranes become very similar. This is because if the shockwave is too strong, then the speed of the water jet is very high; it hits and ruptures the membrane instantaneously without membrane bending and stretching; thus, the results do not depend much on the membrane

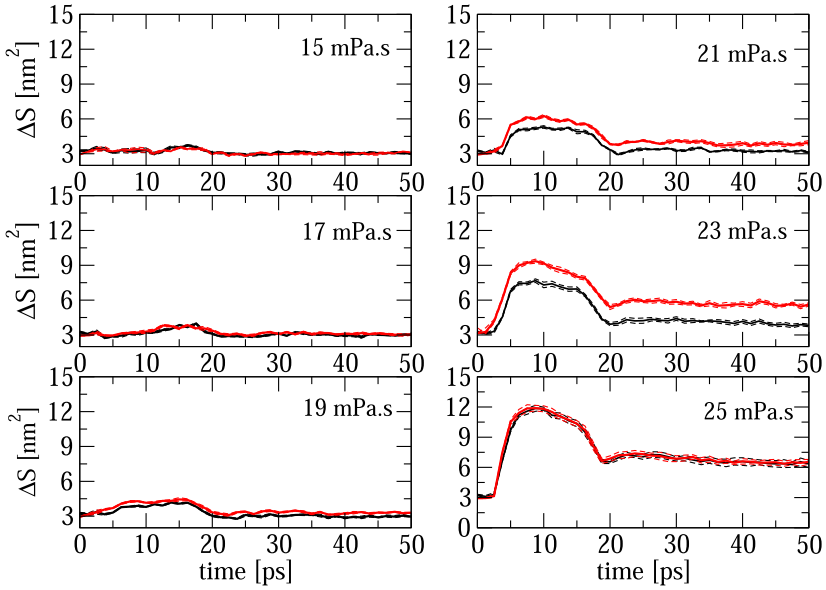

FIG. 7. Time evolution of the pore area ΔS induced by the collapse of a 10 nm bubble under different shockwave impulses I = 15, . . . , 25 mPa s. Results of the normal (black lines) and cancer (red lines) membranes are shown. The average data (over ten trajectories) are shown by the solid thick lines, and the error bars are shown by the dashed lines.

elasticity. Finally, we note that the difference in the average value of ΔS between the two membranes is larger than the standard deviation values, indicating that the cancer membrane is indeed more prone to perforation than the normal membrane.

Next, we wish to investigate the dependence of the pore area on the bubble size, given a shockwave impulse. Figure 8 shows the time evolution of the pore area induced by the collapse of bubbles having diameters d_b = 4–10 nm under a shockwave impulse I = 23 mPa s. This impulse is chosen because the difference in the pore area between the two membranes is most obvious (Fig. 7). We note that in all cases, the shockwave impulse is the same; thus, the pressure exerted by the water jet on the membranes should be the same. However, it is clear that the larger the diameter of the bubble, the larger the diameter of the water jet and therefore the larger the area of the membrane impacted by the water jet. As a consequence, small bubbles with d_b = 4 and 6 nm induce small pores with $\Delta S \sim 3.5$ nm^2, while larger bubbles, d_b = 8 and 10 nm, create larger pore areas. Importantly, given a bubble size, the pore area in the cancer membrane is always larger than that in the normal counterpart. For example, with an 8 nm bubble, the largest pore areas are

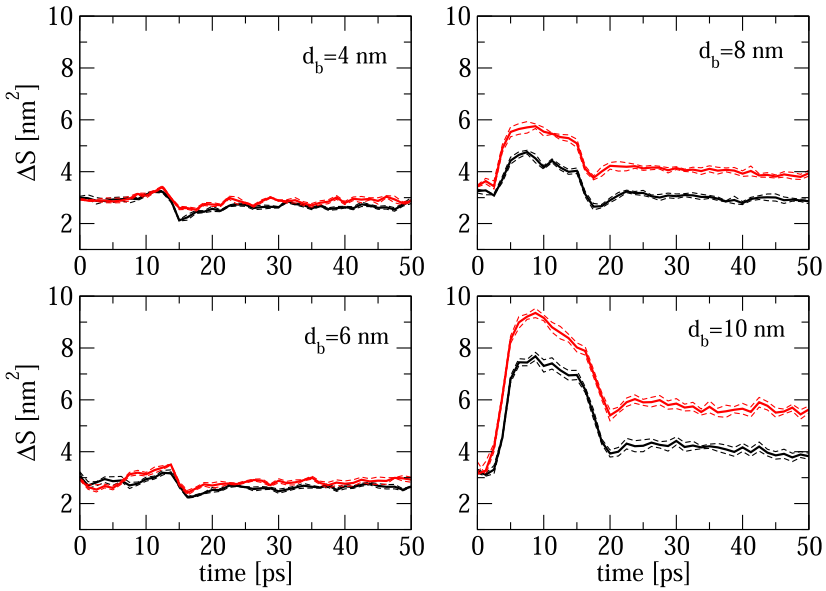

FIG. 8. Time evolution of the pore area induced by the collapse of bubbles with different radius d_b under a shockwave impulse I = 23 mPa s. Results of the normal (black lines) and cancer (red lines) membranes are shown. The average data (over ten trajectories) are shown by the solid thick lines, and the error bars are shown by the dashed lines.

4.5 and 6 nm^2 for the normal and cancer membranes, respectively. After 50 ps, these areas decrease to ~3 and 4 nm^2, indicating that the pore in the normal membrane is closed, but that is still opened in the cancer membrane. Similar results are observed for the 10 nm bubble case (Fig. 8).

In summary, the above results show that (i) given the same bubble, a stronger shockwave impulse induces a larger pore area in the membrane; (ii) for a given shockwave impulse, a larger bubble induces a larger pore in the membrane; (iii) for a given set of the bubble and the shockwave parameters, the pore area in the cancer membrane is always larger than the pore area in the normal membrane; and (iv) if the shockwave impulse is too strong, then the pore areas in the normal and cancer membranes become similar.

C. Pore closure

As shown above, the pore in a membrane induced by a weak shockwave impulse or by the collapse of a small bubble is quickly closed. For example, with a weak impulse of 15 mPa s or a small 4 nm bubble, the pore area reaches the maximum value ~3.5 nm^2 and then quickly decreases to the initial equilibrium value of ~3 nm^2 (Figs. 5 and 8). However, with stronger impulses and/or bigger bubbles, the pore areas are large, and the pore closure is very slow as indicated by slow relaxation of pore area to the initial equilibrium values after 50 ps.

To study the pore closure, we carry out two 100 ns MD simulations under the equilibrium condition with the temperature of 300 K and the pressure of 1 bar for the normal and cancer membranes, starting from structures obtained at 50 ps of the shockwave simulations using the shockwave impulse of 25 mPa s and a 10 nm bubble. The initial pore areas in the normal and cancer membranes are ~6.5 nm (Fig. 7). As seen from Fig. 9, the time evolution of these pore areas under equilibrium condition is quite stable. The pore area in the normal membrane is decreased by ~10%, from 6.5 to 5.8 nm, and that in the cancer membrane is decreased by only 3%, from 6.5 to 6.3 nm after 100 ns (Fig. 9). This suggests that pore closure is rather slow, and importantly, the pore in the normal membrane tends to close more rapidly than the pore in the cancer membrane. To obtain an impression on the closing speed, we simply fit the data between 20 and 100 ns shown in Fig. 9 to a linear function and obtain the closing time of ~1.7 and 5.0 μs for the normal and cancer membranes, respectively. To explain the difference in the timescale of pore closure, we recall that the equilibrium bending modulus of the cancer membrane is smaller (K_c = 8.1 × 10^{-20} J) than that of the normal (K_c = 10.5 × 10^{-20} J) membrane.[26] Therefore, if two membranes are stretched by the same pressure exerted by the water jet, the normal membrane will return to its original state faster than the cancer membrane, assuming that Hooke's law is still valid. Furthermore, we calculate the order parameters, S_i, of lipids from 100 ns equilibrium trajectories after the shockwave excitation and compare results with those obtained from the equilibrium simulation without the shockwave.[26] As seen from Fig. 10, the order parameters of lipids in the normal membrane before and after shockwave excitation are quite similar. In contrast, there are differences in the order parameters, especially of the DOPC and DOPE lipids in the cancer membrane before and after shockwave excitation. This confirms that the cancer membrane relaxes to equilibrium more slowly than the normal membrane.

D. Membrane response under shockwave but no bubble collapse

Finally, to make contact with other works, we consider the impact of shockwaves alone, i.e., without the bubble (d_b = 0 nm). To this end, we perform simulations using a relatively strong shockwave with the impulse of 23 mPa s. Figures 11(a) and 11(b) show snapshots of the normal and cancer membranes, respectively, at t = 3 ps when the shockwave just hits the membrane. As seen, the membranes are hardly affected, i.e., no bending or poration

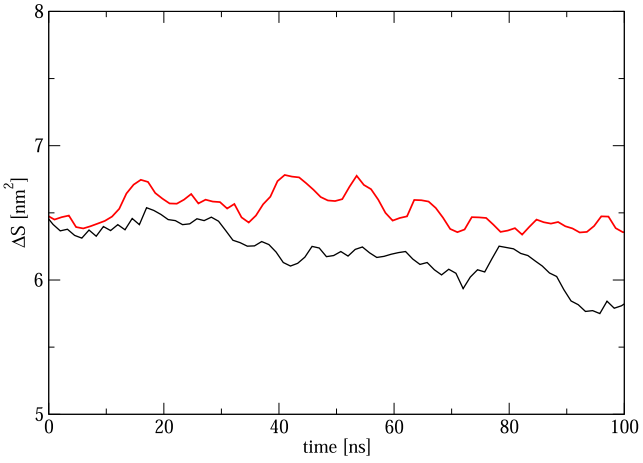

FIG. 9. Time evolution of the pore area in the normal (black line) and cancer (red line) membranes under the equilibrium condition at 300 K and 1 bar. The initial pores at t = 0 ns were perforated by a shockwave impulse of 25 mPa s and a 10 nm bubble.

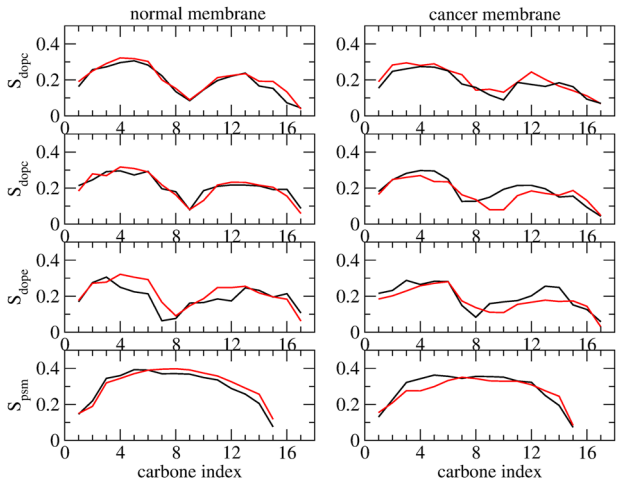

FIG. 10. The order parameters averaged over the two tails sn-1 and sn-2 of four lipid types: DOPC, DOPE, DOPS, and PSM, of the normal (left panels) and cancer (right panels) membranes. Carbon atom numbers increase in the direction of the tail termini. Results before (black) and after (red) the shockwave induced bubble collapse are shown.

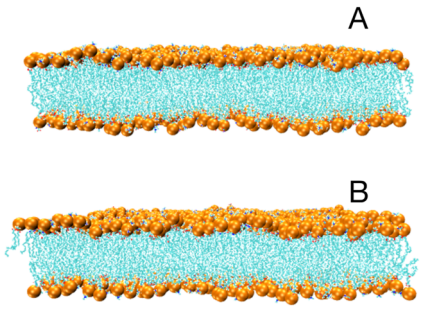

FIG. 11. Snapshots taken at $t = 3$ ps from the simulation of the normal (a) and cancer (b) membranes without the bubble but with a shockwave impulse of 23 mPa s. The phosphate atoms of lipids are shown in orange, and the other atoms are shown in cyan.

is observed. We increase the shockwave impulse up to 30 mPa s, but similar results are obtained. This indicates that the shockwave alone does not induce significantly structural changes in the membranes, in agreement with previous studies.[12,18,20,38,39] Furthermore, the response of the normal and cancer membranes to the shockwave is similar.

IV. DISCUSSION

We perform MD simulations of the shockwave induced bubble collapse to investigate the difference in the response of the normal and cancer cell membranes. These two membranes are different in the elastic moduli, caused by the difference in the concentration of the phosphatidylserine lipids in the outer leaflet and the cholesterol in the bilayer.[26]

We first discuss the impact of shockwaves alone on two membranes. Under the shockwave excitation, a water flow is generated and uniformly directed toward the membrane, exerting a uniform pressure across all locations on the membrane; therefore, the membrane is simply compressed but not perforated. Indeed, Berkowitz and colleagues performed shockwave induced bubble collapse simulations of a DPPC lipid membrane using the MARTINI coarse-grained lipid model and showed that a high intensity shockwave with an impulse of 18 mPa s does not induce pores in the membrane.[18] Similarly, the simulation of Wei *et al.* for a single-component DOPC lipid membrane using the MARTINI force field showed slight compression of the membrane and no pores formation.[23] Lu *et al.*[20] and Wang *et al.*[39] studied DPPC lipid membranes using the all-atom GROMOS force field[40] and showed that the membranes are not perforated under the shockwave alone. Our simulations of multi-component lipid membranes using the all-atom CHARMM36 force field show that shockwaves alone do not induce pore formation, confirming previous studies using different lipid models, compositions, and force fields.[18,20,23,39] However, all these results contradict the result of Espinosa *et al.* who showed that a shockwave alone with an impulse of ~0.45 mPa s could damage the membrane to an unrecoverable state.[38] This could be due to the very small size membrane studied by Espinosa *et al.*[38]

The presence of a bubble is essential for pore formation because it focuses the uniform water flow generated by the shockwave into a water jet, which hits the membrane at a focal area. The peak pressure values at this area are very high, for example, up to 4.2 GPa in the simulation with $I = 21$ mPa s and 10 nm bubble, which can perforate pores at the focal area. Using the piston method to generate the shockwave,[41] Adhikari *et al.* showed that the peak pressure at the membrane is ~0.55 GPa in a simulation using a piston velocity of 1 km/s and a 60 nm bubble.[18] Ganzenmueller *et al.* performed large scale coarse-grained simulations with a piston velocity of 4.73 km/s but without a bubble and showed that the peak pressure is ~3 GPa.[12] In all these studies, although the peak pressure values are very high but the durations of the shockwaves are very short, therefore, the values of the pressure impulses exerted on the membrane are very small (Table II). We should mention that these values are much lower than an experimentally measured value impulse of 54 Ps s, which is sufficient to deliver calcein molecules into the cell but does not cause the cell death.[42]

We then study the response of the membrane as a function of the shockwave impulse and bubble size in detail. Overall, our results show that the stronger the shockwave impulse or the larger the size of the bubble, the larger the pore area. This result is similar to the earlier simulations of Wei *et al.*[23] and Sun *et al.*[19] although the authors used a different, i.e., momentum mirror method to generate the shockwave, and moreover, the system sizes, lipid compositions, and the force fields are different from our simulations.

The cancer membrane studied in this work has a lower bending modulus than the normal counterpart. As a consequence, for a given shockwave impulse and bubble combination, the cancer membrane is more bent and perforated than the normal membrane. The pore area in the cancer membrane is always larger than the pore area in the normal membrane. However, we do not observe extreme cases where the cancer membrane was perforated, while the normal membrane was not. This is because the bending modulus of the cancer membrane is only ~22% smaller than that of the normal membrane; thus, the response of two membranes to the water jet is not much different. The largest differences of 20%–23% in the pore areas between the normal and cancer membranes are observed for the cases with the shockwave impulses of 21–23 mPa s and a bubble of 10 nm. We observe that increasing the shockwave impulse and/or bubble size to large values does not increase the difference in the pore area. This is because the pressure exerted by the water jet on the membrane is too strong, lipids are immediately expelled from the membrane, and pores are formed without much bending of the membrane. This means that in this case, the difference in the elasticity between the normal and cancer membranes does not really determine the difference in the pore areas. We show that the pore formed in the cancer membrane is closed more slowly than the pore in the normal membrane, implying that once deformed, the cancer membrane takes longer to relax to equilibrium than the normal cell membrane. Again, this is because the cancer membrane has a lower bending modulus than the normal counterpart.

As mentioned, there have been a number of simulation studies on the interaction between the shockwave and membranes.[10,11,16–23,39] However, to our best knowledge, there is currently only one simulation of Wei *et al.* who studied the response of membranes with different elasticities on the shockwave induced bubble collapse. In that work, the membrane is a single-component DOPC lipid bilayer modeled by the coarse-grained MARTINI force

field. The elasticity of the DOPC membrane is varied by varying the population of the peroxidized DOPC lipids. The bending modulus of the 100% peroxide lipid membrane is $K_c = 4.3 \times 10^{-20}$ J, which is about half of that of the membrane without peroxide, $K_c = 8.4 \times 10^{-20}$ J. As a consequence, the authors showed that a shockwave impulse of 127.1 mPa s is required to perforate the 100% peroxide membrane, while a stronger impulse of 161.3 mPa s is necessary for the pore formation in the 0% peroxide membrane. This result together with our result confirms that the shockwave induced bubble collapse damage threshold for low elastic membranes is lower than that required for high elastic counterparts.

It is instructive to compare the timescale of pore formation induced by the shockwave induced bubble collapse with that obtained by other excitation methods. In a previous study, we simulated the effect of stable bubble cavitation on a lipid bilayer and showed that the bubble fuses with the membrane and subsequent cavitation pulls lipid molecules out of the membrane, creating pores after ~30 ns.[32] In another work, we simulated the direct interaction between focused ultrasound and a lipid membrane and showed that the spatial pressure gradient between the focused and non-focused regions causes the pore formation after ~225 ns.[43] If the pore opening process is slow, then unwanted molecules may be able to enter the cell together with drugs during the pore opening. In this context, the shockwave method is preferable because it allows for a rapid drug delivery into cells.

The simulation does not show large differences in the pore areas in the normal and cancer membranes because the bending moduli of two membrane models are not much different. Is this true for real biological cells? In reality, cancer cells are much softer than normal cells.[24] For example, Lekka *et al.* used scanning force microscopy to examine the elasticity of normal and cancer human bladder cells, and the results show that Young's modulus, defined as a measure of cellular deformability, of cancer cells is one order of magnitude larger as compared to healthy cells.[44] Using high-throughput optical tweezers technique, three cell lines were compared: non-tumorigenic breast epithelial MCF10 cells, non-motile, non-metastatic breast epithelial cancer MCF7 cells, and MCF7 cells transformed with phorbol ester. The results showed a significant increase in the deformability in the transformed MCF7 cells as compared to both non-metastatic MCF10 and non-transformed MCF7 cells.[45] Further studies provide a large database of cases, showing significantly larger deformability of single cancer cells.[46–48] The very large difference in the elasticity between normal cells and cancer cells suggests that one can always be able to select a suitable range of parameters of the shockwave impulse and bubble such that cancer cells are maximally perforated, while normal cells are minimally affected or even unaffected. Even if the normal cell is perforated, the pores will be closed more quickly; therefore, if drugs are injected after the pores in the normal cells have closed, then drugs can only enter the cancer cells where pores are still open, i.e., the normal cells are safe.

We acknowledge that although this is a proof-of-concept work, we believe that our proposed method can be realized experimentally. Indeed, shockwaves have been applied to cancer therapy. Some experimental works have shown that the shockwave can suppress tumor growth and selectively kill malignant cells.[15,49] The technique that uses a laser-induced shockwave to drive a liquid microjet at a very speed has also been developed.[50] The gas bubbles have been widely used in ultrasound induced bubble cavitation, aimed at enhancing drug delivery into cells. In this approach, ultrasound is used to induce the stable cavitation of microbubbles, generating microstreaming, which exerts shear stresses on the cell membrane, resulting in pore formation or even disruption of the cell.[51] In this context, the combination of shockwaves and bubbles into an experimental method to rapidly and selectively perforate cancer cell membranes for drug delivery is quite doable.

V. CONCLUSION

We have performed MD simulations of the shockwave induced bubble collapse on normal and cancer membrane models. We showed that the combination of shockwaves and bubbles is essential for the pore formation in the membrane. That is, the perforation is due to the water nanojet generated by a collapse of bubbles under shockwaves. We showed that given a combination of a shockwave and a bubble, the cancer membrane is more bent, and the pore area in the cancer membrane is larger than that in the normal membrane because the cancer membrane is softer than the normal membrane. However, the pore areas in the two membrane types become similar if the shockwave is too strong. Our simulation results could provide a proof-of-concept for the development of a new method that uses shockwaves and bubbles to rapidly deliver drugs into cancer cells, while leaving normal cells less affected. For further development, it is important to obtain the pore area as a function of the bending modulus for various cancer cell membranes, which have different elastic properties. This could provide a hint for optimizing the shockwave impulse and bubble size in order to optimize the drug delivery outcome. Finally, we noted that the cell membranes considered in this work contain only lipid bilayers. It is necessary to include other components, such as cytoskeleton, which is responsible for providing structural integrity and mechanical stability. To model such complex systems, one could resort to advanced multiscale, coarse-grained approaches.[12–15] This is our future research direction.

ACKNOWLEDGMENTS

This work was supported by the Department of Science and Technology at Ho Chi Minh City, Vietnam (Grant No. 13/2020/HD-PQTKHCN), the European Union's Horizon 2020 Research and Innovation Program under Marie Skłodowska-Curie Grant Agreement No. 101034407, and the CNRS. We acknowledge the computational support from the IDRIS, CINES, and TGCC centers (Project No. A0110712955). This work has been also supported by the National Science Centre, Poland (grant 2019/35/B/ST4/02086).

AUTHOR DECLARATIONS

Conflict of Interest

The authors have no conflicts to disclose.

Author Contributions

Nguyen Hoang Linh: Methodology (equal). **Viet Hoang Man**: Methodology (equal). **Mai Suan Li**: Funding acquisition (equal). **Junmei Wang**: Funding acquisition (equal). **Philippe Derreumaux**: Writing – review & editing (equal). **Thi Ly Mai**: Formal analysis

(equal). **Phuong H. Nguyen**: Conceptualization (equal); Data curation (equal); Formal analysis (equal); Funding acquisition (equal); Investigation (equal); Methodology (equal); Project administration (equal); Resources (equal); Software (equal); Supervision (equal); Validation (equal); Visualization (equal); Writing – original draft (equal); Writing – review & editing (equal).

DATA AVAILABILITY

The data that support the findings of this study are available from the corresponding author upon reasonable request.

REFERENCES

[1] S. D. Conner and S. L. Schmid, Nature **422**, 37 (2003).
[2] P. Shinde, A. Kumar, Kavitha, K. Dey, L. Mohan, S. Kar, T. K. Barik, J. Sharifi-Rad, M. Nagai, and T. S. Santra, Delivery Drugs **2**, 161 (2020).
[3] P. Tyagi and Y.-C. Chuang, Transl. Res. Biomed. **6**, 117 (2018).
[4] T. Kodama, A. G. Doukas, and M. R. Hamblin, Biochim. Biophys. Acta **1542**, 186 (2002).
[5] L. M. López-Marín, B. E. Millán-Chiu, K. Castaño-González, C. Aceves, F. Fernández, A. Varela-Echavarría, and A. M. Loske, J. Membr. Biol. **250**, 41 (2017).
[6] B. Qi, T. Yu, C. Wang, T. Wang, J. Yao, X. Zhang, P. Deng, Y. Xia, W. G. Junger, and D. Sun, J. Exp. Clin. Cancer Res. **35**, 161 (2016).
[7] U. Lauer, E. Bürgelt, Z. Squire, K. Messmer, P. Hofschneider, M. Gregor, and M. Delius, Gene Ther. **4**, 710 (1997).
[8] R. Murata, K. Nakagawa, S. Ohtori, N. Ochiai, M. Arai, T. Saisu, T. Sasho, K. Takahashi, and H. Moriya, Osteoarthritis Cartilage **15**, 1275 (2007).
[9] G. Yao, J. Chen, Y. Duan, and X. Chen, BioMed Res. Int. **2020**, 2064781.
[10] K. Koshiyama, T. Kodama, T. Yano, and S. Fujikawa, Biophys. J. **91**, 2198 (2006).
[11] A. Choubey, M. Vedadi, K.-i. Nomura, R. K. Kalia, A. Nakano, and P. Vashishta, Appl. Phys. Lett. **98**, 023701 (2011).
[12] G. C. Ganzenmueller, S. Hiermaier, and M. O. Steinhauser, Soft Matter **7**, 4307 (2011).
[13] G. C. Ganzenmueller, S. Hiermaier, and M. O. Steinhauser, PLoS One **7**, e51989 (2012).
[14] M. Schmidt, U. Kahlert, J. Wessolleck, D. Maciaczyk, B. Merkt, J. Maciaczyk, J. Osterholz, G. Nikkhah, and M. O. Steinhauser, Sci. Rep. **4**, 3849 (2014).
[15] M. O. Steinhauser and M. Schmidt, Soft Matter **10**, 4778 (2014).
[16] K. P. Santo and M. L. Berkowitz, J. Phys. Chem. B **119**, 8879 (2014).
[17] K. P. Santo and M. L. Berkowitz, J. Chem. Phys. **140**, 054906 (2014).
[18] U. Adhikari, A. Goliaei, and M. L. Berkowitz, J. Phys. Chem. B **119**, 6225 (2015).
[19] D. Sun, X. Lin, Z. Zhang, and N. Gu, J. Phys. Chem. C **120**, 18803 (2016).
[20] X.-m. Lu, B. Yuan, X.-r. Zhang, K. Yang, and Y.-q. Ma, Appl. Phys. Lett. **110**, 023701 (2017).
[21] N. Nan, D. Si, and G. Hu, J. Chem. Phys. **149**, 074902 (2018).
[22] Q. Hu, L. Zhang, and R. P. Joshi, AIP Adv. **9**, 045006 (2019).
[23] T. Wei, L. Gu, M. Zhou, Y. Zhou, H. Yang, and M. Li, J. Phys. Chem. B **125**, 6912 (2021).
[24] C. Alibert, B. Goud, and J.-B. Manneville, Biol. Cell **109**, 167 (2017).
[25] F.-S. Quan and K. S. Kim, Acta Biochim. Biophys. Sin. **48**, 865 (2016).
[26] N. H. Linh, V. H. Man, M. S. Li, J. Wang, P. Derreumaux, and P. H. Nguyen, Phys. Chem. Chem. Phys. **24**, 6225 (2022).
[27] D. Marquardt, B. Geier, and G. Pabst, Membranes **5**, 180 (2015).
[28] J. Connor, C. Bucana, I. J. Fidler, and A. J. Schroit, Proc. Natl. Acad. Sci. U. S. A. **86**, 3184 (1989).
[29] T. Utsugi, A. J. Schroit, J. Connor, C. D. Bucana, and I. J. Fidler, Cancer Res. **51**, 3062 (1991).
[30] K. Simons and E. Ikonen, Science **290**, 1721 (2000).
[31] H. Fu, J. Comer, W. Cai, and C. Chipot, J. Phys. Chem. Lett. **6**, 413 (2015).
[32] V. H. Man, P. M. Truong, M. S. Li, J. Wang, N.-T. Van-Oanh, P. Derreumaux, and P. H. Nguyen, J. Phys. Chem. B **123**, 71 (2019).
[33] A. D. MacKerell, Jr., D. Bashford, M. Bellott, R. L. Dunbrack, J. D. Evanseck, M. J. Field, S. Fischer, J. Gao, H. Guo, S. Ha, D. Joseph-McCarthy, L. Kuchnir, K. Kuczera, F. T. K. Lau, C. Mattos, S. Michnick, T. Ngo, D. T. Nguyen, B. Prodhom, W. E. Reiher III, B. Roux, M. Schlenkrich, J. C. Smith, R. Stote, J. Straub, M. Watanabe, J. Wiórkiewicz-Kuczera, D. Yin, and M. Karplus, J. Phys. Chem. B **102**, 3586 (1998).
[34] E. Lindahl, B. Hess, and D. van der Spoel, J. Mol. Model. **7**, 306 (2001).
[35] T. Darden, D. York, and L. Pedersen, J. Chem. Phys. **98**, 10089 (1993).
[36] O. H. Ollila, H. J. Risselada, M. Louhivuori, E. Lindahl, I. Vattulainen, and S. J. Marrink, Phys. Rev. Lett. **102**, 078101 (2009).
[37] L. S. Vermeer, B. L. de Groot, V. Réat, A. Milon, and J. Czaplicki, Eur. Biophys. J. **36**, 919 (2007).
[38] S. Espinosa, N. Asproulis, and D. Drikakis, Microfluid. Nanofluid. **16**, 613 (2013).
[39] X.-f. Wang, G. Tao, P. Wen, B.-x. Ren, C.-q. Pang, and C.-x. Du, J. Phys. Chem. B **124**, 9535 (2020).
[40] W. van Gunsteren, S. R. Billeter, A. A. Eising, P. H. Hünenberger, P. Krüger, A. E. Mark, W. Scott, and I. Tironi, *Biomolecular Simulation: The GROMOS96 Manual and User Guide* (VDF Hochschulverlag AG an der ETH, Zurich, 1996).
[41] P. Wen, G. Tao, D. E. Spearot, and S. R. Phillpot, J. Appl. Phys. **131**, 051101 (2022).
[42] T. Kodama, M. R. Hamblin, and A. G. Doukas, Biophys. J. **79**, 1821 (2000).
[43] V. H. Man, M. S. Li, J. Wang, P. Derreumaux, and P. H. Nguyen, J. Chem. Phys. **150**, 215101 (2019).
[44] M. Lekka, P. Laidler, D. Gil, J. Lekki, Z. Stachura, and A. Z. Hrynkiewicz, Eur. Biophys. J. **28**, 312 (1999).
[45] J. Guck, S. Schinkinger, B. Lincoln, F. Wottawah, S. Ebert, M. Romeyke, D. Lenz, H. M. Erickson, R. Ananthakrishnan, D. Mitchell, J. Käs, S. Ulvick, and C. Bilby, Biophys. J. **88**, 3689 (2005).
[46] E. C. Faria, N. Ma, E. Gazi, P. Gardner, M. Brown, N. W. Clarke, and R. D. Snook, Analyst **133**, 1498 (2008).
[47] W. Xu, R. Mezencev, B. Kim, L. Wang, J. McDonald, and T. Sulchek, PLoS One **7**, e46609 (2012).
[48] M. Lekka, D. Gil, K. Pogoda, J. Dulińska-Litewka, R. Jach, J. Gostek, O. Klymenko, S. Prauzner-Bechcicki, Z. Stachura, J. Wiltowska-Zuber, K. Okoń, and P. Laidler, Arch. Biochem. Biophys. **518**, 151 (2012).
[49] F. Gamarra, F. Spelsberg, M. Dellian, and A. E. Goetz, Int. J. Cancer **55**, 153 (1993).
[50] V. Menezes, S. Kumar, and K. Takayama, J. Appl. Phys. **106**, 086102 (2009).
[51] G. Peruzzi, G. Sinibaldi, G. Silvani, G. Ruocco, and C. M. Casciola, Colloids Surf., B **168**, 83 (2018).